PHOTO-TUNABLE DYNAMICS STUDIES ON SOLITONIC STRUCTURES IN CHIRAL NEMATIC LIQUID CRYSTALS

Changda Liu

Department of Physics

10/18/2018, 10:50 a.m. at Duane F1117

Committee member: Ivan Smalyukh (Thesis Advisor, Physics), John Cumalat (Physics), David Walba (Chemistry), Susan Hendrickson (Chemistry)

Abstract

Rich dynamic behavior of solitons has attracted a great deal of interest in fields of physics ranging from fluid dynamics to optics. Unlike in those fields, topological solitons are extremely accessible when using liquid crystals as a host medium, providing a model experimental system for discovering the physics behind. The research presented in this thesis studied the photo-tunable dynamics of a topological solitonic field configuration dubbed “torons” in chiral nematic liquid crystals, and we show that precise-controlling of the toron motions, forming reconfigurable lattice-structures of torons, and potentially controlling the electric-driven toron “squirming” motions, can be achieved with light exposure.

Acknowledgements

I would like to thank professor Smalyukh for providing me with the opportunity to work on this project and for guiding me in my experimental endeavors. I would also like to thank Hayley R. O. Sohn, who cooperated with me on this project and provided me with so much help every step of the way. In addition, I would like to thank everyone in the Smalyukh research group for their assistance with the lab equipment and for granting me time to conduct my research in the lab.

Contents

1. Introduction

1.1 Liquid Crystals

As of today, with the help of our constantly-evolving theoretical understanding and experimental skills, liquid crystals (LCs) serve as a great tool to make technologies from a variety of fields possible. A LC is a phase of matter between solid and liquid, which can be achieved by heating a specific crystalline material past its melting point but not letting the liquid become isotropic, or through inorganic solutions of amphiphilic molecules [1]. LCs share some properties of both liquid and solid, giving rise to fluidity while maintaining the anisotropy in optical properties and periodic arrangement of molecules in one spatial direction [2], just like crystals.

There are many types of LCs. To fully understand this, here we introduce the concept of director field $\mathbf{n}(\mathbf{r})$, which is made up of unit vectors that represent the average LC molecule orientation with head-tail symmetry. The simplest phase of LCs is the nematic liquid crystal (NLC), where the rod-shaped molecules tend to have long-range orientations, in other words the molecules will point in the same direction (see Fig.1(a)). The cholesteric phase, in contrast to the nematic phase, has a spontaneous macroscopic helical structure with a twist axis perpendicular to the local director. Thus the chiral phase consists of local nematic "layers", which are continuously twisted with respect to each other [3] (see Fig.1(b)) [4]. The period of this variation (the distance over which a full rotation of 2π is completed) is known as the pitch, p.

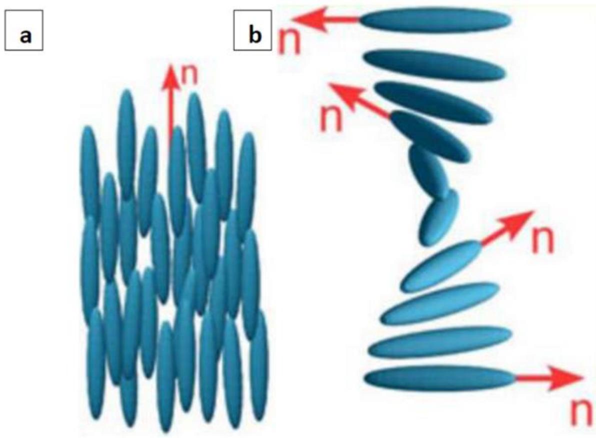

Figure 1 | (**a**) The nematic liquid crystal phase. The molecules are all oriented in a single direction, however, the molecules themselves have no positional order. Each molecule points vertically resulting in a director along the n-axis. (**b**) The cholesteric liquid crystal phase. The molecules exhibit twist along the vertical axis. The distance shown in this diagram is half of the material's pitch. Image taken from [4].

The chiral nematic liquid crystals (CNLCs) are formed from liquid crystal materials possessing inherent chirality (e.g., cholesterols) or by addition of a chiral dopant into a nematic liquid crystal host. This research is mainly associated with the cholesteric LCs that are prepared by mixing a room-temperature nematic host with a chiral additive.

1.2 Solitons and Topologies

In mathematics and physics, a soliton is a self-reinforcing solitary wave packet that maintains its shape while it propagates at a constant velocity. These solitons typically emerge from a delicate balance of nonlinear and dispersive effects in the physical host medium [5], and their rich dynamic behavior has attracted a great deal of interest. Solitons are the solutions of non-linear dispersive partial differential equations describing not only wave propagation but also other physical systems. The huge amount of information on nonlinear wave phenomena obtained through the collaboration of mathematicians and physicists makes the soliton concept one of the most significant developments in modern mathematical physics [6].

Solitons of a very different type, often called "topological solitons", are topologically-nontrivial, spatially-localized nonsingular field configurations that are rarely associated with out-of-equilibrium dynamics, but rather are studied as static field configurations embedded in a uniform background [7]. In particle physics, topological solitons – now dubbed "skyrmions" – are topologically stable field configurations. Skyrmions are important in solid state physics, especially in the emerging technology of spintronics, and they also have ties to certain areas of the string theory. A skyrmion is roughly understood to be a localized variation in the field, in which $\mathbf{n}(\mathbf{r})$ rotates continuously through an angle π or $\pi/2$ (in the case of a half-Skyrmion) from its center to its boundary. Figure 2(a) illustrates the vector field profile of a half-Skyrmion [8]. Similarly, double-twist cylinders exhibit 2-D twist in the directions perpendicular to the cylindrical axis (see Fig.2(b)) [9].

Figure 2 | Images taken from [9]. (**a**) A half-skyrmion excitation illustrated from two different viewing directions. The cylinders describe the director *n*. (**b**) A double-twist cylinder. The director field twists in all directions perpendicular to the vertical axis of the double-twist cylinder

In LCs, topological solitons realized in localized configurations of the director field $\mathbf{n}(\mathbf{r})$ known as elementary "torons" [10] contain skyrmionic configurations in the two-dimensional cross-sectional midplane. [11]. By means of local energetic excitation, a confined cholesteric can self-assemble into a toroidal structure, which can be visualized as a double-twist cylinder looped onto itself (Fig.3). The director field twists π radians from the center to the outside of the toron. At the center, the director field is vertically aligned, perpendicular to the plane of the cylindrical axis. As a result of this configuration, two point defects appear along the vertical axis of the toron near the substrate surfaces and help to embed this configuration in the surrounding, vertically aligned liquid crystal (see Fig.3(c), (d)) [12].

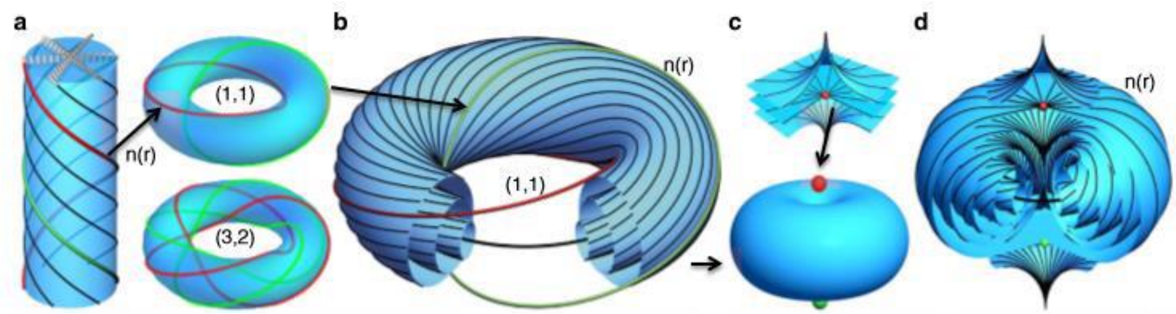

Figure 3 | (**a**) A double-twist cylinder. (**b**) A double-twist torus (toron) formed by a double-twist cylinder looped on itself. (**c**) Hyperbolic defects of charge +/- 1 that are above and below the torus in uniform homeotropic far field that enable the loop of double twist to meet the vertical surface boundary conditions. (**d**) The director field structure of the toron. Images taken from [12].

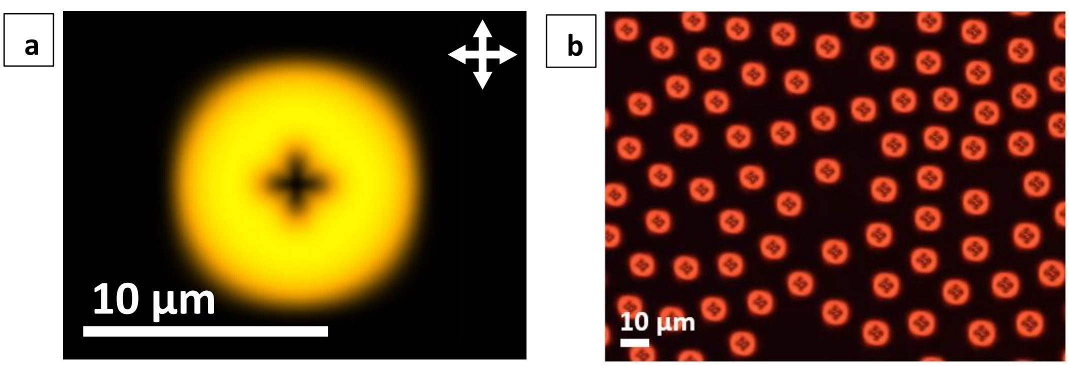

Figure 4 | (**a**) A computer-simulated image of a single toron between two crossed polarizers (shown by white double arrows) with a comparing length of 10 µm. (**b**) An array of torons in experiment between two crossed polarizers taken under an Olympus BX51 microscope with a comparing length of 10 µm.

In summary, there is a four-fold relationship between the concepts we've discussed: (1) topological solitons are solitons of a different kind from what is typically discussed in nonlinear physics, (2) skyrmions are interesting topological solitons in particle physics, (3) the stability of the twisted toron structures in LCs is mediated by the CNLC's tendency to twist, and (4) torons are skyrmionic field configurations in CNLCs with a skyrmion number of 1. In many fields of physics, solitons are nearly impossible to generate, while topological solitons are extremely accessible when using LCs as a host medium. Therefore, as long as we understand and characterize the properties of torons in LCs, we could essentially apply the knowledge to solitons in other fields and potentially benefit many aspects of physics research.

1.3 Dynamics of Torons

Earlier we introduced the concept of pitch p (distance over which the director field twists around the helical axis by 2π radians). Mathematically, the pitch is defined as $p = 1/h_{HTP}C_{chiral}$ [10, 13], where h_{HTP} represent the known value "helical twisting power", and C_{chiral} denotes the concentration of the chiral dopant. As local and global minima of free energy, the torons occur spontaneously in cells with d/p = 1, where d is the separation of the two confining glass substrates of the sample [14]. In other words, torons as field configurations are more stable and energetically favorable when the environment has suitable sample thickness over pitch ratio, d/p.

For free energy considerations, since the torons are more energetically favorable with a certain d/p ratio, changing the ratio within a localized area would essentially force the torons to move away from the area to find the more favorable original d/p. Because the sample thickness is unchangeable once the sample has been made, as long as we are able to induce a gradient change in pitch in the cell, we could induce dynamics of torons.

Changes in pitch can be induced with electric field, heat, or light with advantages and disadvantages associated with each. Usually the most studied approach has been electro-optic in systems made up of "static" chiral dopants [15], and previous work in my research group has also demonstrated that directional electrical driven motion of torons can be exhibited while applying moderate electric tuning.[12,13,14] On the other hand, an increasingly common means for fabricating dynamic, tunable CNLC devices is to photosensitize the chiral dopant. This approach can overcome some of the hurdles associated with electro-optic CNLC devices while also extending application considerations [15]. The photosensitizing process will be discussed later in Section 2.

1.4 Thesis Overview

In this research, we will be focusing on investigating and precisely controlling the photo-tunable dynamics of torons in CNLCs. The following sections will discuss the procedures and results of the experiments and compare the results to related research. This paper will also provide potential applications and future plans for the project.

2. Methods

2.1 Sample Preparations and Experiment Setup

Essentially, two types of LC samples were used for the experiments. All samples consisted of a nematic host (either 5CB or MLC-6609) mixed with a photo-tunable chiral dopant called QL76, which is a axially chiral bis(azo) molecule with a high-helical-twisting power (*HTP*) in the *trans/trans* state (60 μm^{-1}) and a lower *HTP* in the *cis/cis* state (27 μm^{-1}) [15]. Figure 5(a) below shows the basic chemical structure of the QL76 molecules. The usually-high *HTP* of these azo-containing axially chiral dopants can be reduced with a *trans/trans* to *cis/cis* isomerization by UV-light exposure. Since pitch is defined as ($p = 1/h_{HTP}C_{chiral}$), the photo-directed change in *HTP* of QL76 would allow variance across a wide range of pitch, which enables the photo-tunable dynamics of torons as described earlier. For the toron size-dependence experiments (Section 2.2.1), toron controllable directional motion experiments (Section 2.2.2), and the toron Lattice-Structure

(Section 2.2.3), the nematic host 5CB (positive dielectric anisotropy) was used and

e labeled IQ1-4 with different thickness and pitch. For the “Squirming Motion under Light Exposure” experiments (Section 2.2.4), the nematic host MLC-6609, which has negative dielectric anisotropy, was used.

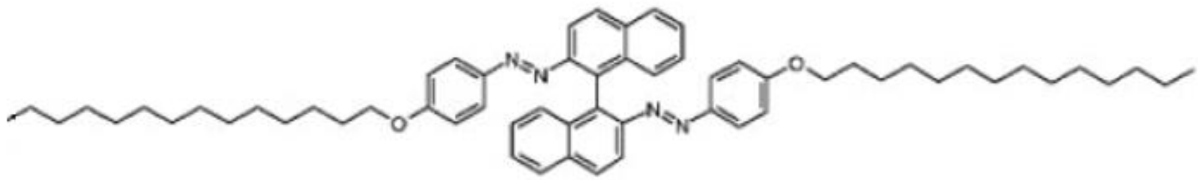

Figure 5 | The basic chemical structure of a QL76 molecule.

As for general sample preparation, the samples were constructed with two glass substrates and mounted on microscope slides. To impose strong homogeneous vertical surface boundary conditions for the LC samples, Polyimide SE-1211 was applied to the glass substrates with transparent indium tin oxide (ITO) electrodes via spin coating at 2700 rpm for 30 s, then baked for 5 min at 90 °C and 1 h at 190 °C. Glass fiber segments dispersed in ultraviolet-curable glue were sandwiched between the two glass substrates as spacers to set the inter-substrate separation gap, or sample thickness, d. The CNLC materials were filled into the confinement cells by means of capillary forces and the edges of the cells were then sealed with 5-min fast-setting epoxy.

Leads were soldered to the ITO electrodes to provide electrical connection across the LC cells. For “squirming” motions under light exposure experiments, a homemade MATLAB-based function generator coupled with a data acquisition board (NIDAQ-6363, National Instruments) was used to produce square-waves of different frequency and voltage, which were applied to the samples via the soldered leads.

A pair of optical tweezers, consisting of a 1064 nm ytterbium-doped fiber laser (YLR-10-1064, IPG Photonics) controlled by a homemade LabView program, were used to generate torons by means of optically-induced local reorientation, a process in which the LC director couples to the optical-frequency electric field of the laser beam and realigns away from the far-field background **n**(**r**) [13]. The output power was usually controlled between 20 mW to 28 mW for a case-to-case basis for different samples to "draw" mobile torons (too much power would result in generating "pinned" torons and power over 50 mW could melt the LCs to the isotropic phase).

We used an Olympus BX-51 upright microscope, with crossed polarizers inserted above and below the sample, and a 10x objective for observations of the experiments. A simple projecting system consisting of an Epson projector and a few reflecting mirrors for alignment purposes was connected to the BX-51 microscope, enabling light patterns to be projected onto the samples under the microscope. Transmission-mode polarizing optical microscopy (POM) images and videos were captured/recorded via a CCD (charge-coupled device) camera (Flea, PointGrey). The videos and images were then put in open-source software ImageJ/FIJI (available via the National Institute of Health). We used the software's particle-tracking capabilities to analyze the toron dynamics, and the extracted data was further analyzed in MATLAB for velocity and trajectory information.

2.2 Experiments

2.2.1 Toron Size-dependence

2.2.1.1 Experiments

As a reminder, we have discussed earlier that theoretically torons as topological solitonic structures in LCs tend to move away from changed pitch ($p = 1/h_{HTP}C_{chiral}$) to maintain the energetically favorable d/p ratio. We start with a toron size-dependence experiment with a uniform light exposure onto the samples to better understand how torons react to light-induced pitch changes.

The total LC free energy can be described as the Frank-Oseen equation below:

$$W = \int \left[\frac{K_{11}}{2}(\nabla \cdot \boldsymbol{n})^2 + \frac{K_{22}}{2}\ (\boldsymbol{n} \cdot \nabla \times \boldsymbol{n} + q_0)^2 + \frac{K_{33}}{2}(\boldsymbol{n} \times \nabla \times \boldsymbol{n})^2 - \frac{\varepsilon_0 \Delta\varepsilon}{2}(\boldsymbol{E} \cdot \boldsymbol{n})^2\right] dV \qquad (1)$$

where K_{11}, K_{22}, and K_{33} are the elastic constants representing the energetic cost for splay, twist, and bend deformations. q_0 is the chiral wave number of the ground-state chiral nematic mixture and is defined as: $q_0 = 2\pi/p_0$. According to Figure 6, when the QL76 molecules are at the exposed state (cis/cis), the value of q_0 is smaller compared to the ground state. Thus, if we shine light onto the samples to expose QL76 molecules (from red line to green line), q_0 decreases, which means in equation (1) we are lowering the twist free energy and thus changing the entire free energy landscape of the sample (see Fig.7). Therefore, for uniform exposure of light, since there is no area with a favorable d/*p* ratio for the exposed torons to run to, in theory these torons would not move but instead change size to fulfill the twist free energy to adjust to the new d/*p*. After the projection is taken away, the system would quickly relax back to the ground state and return to the original d/*p*, in this case the torons should slowly grow back to their original size from the "exposed size" (see Fig.8).

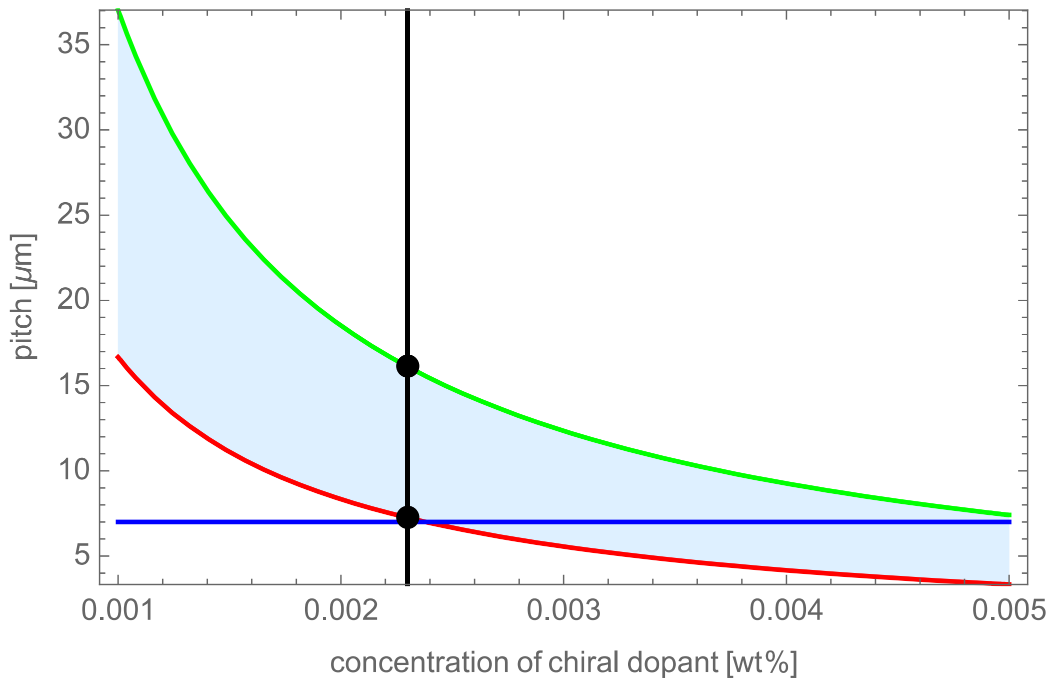

Figure 6 | A simulated plot of pitch vs. the concentration of chiral dopant C_{chiral}. Note that the red line denotes the ground-state of the system, and the green line represents the excited state. A vertical solid black line is shown crossing the two states at $C_{chiral} = 0.23\%$, which is the concentration of the QL76 in our LC samples.

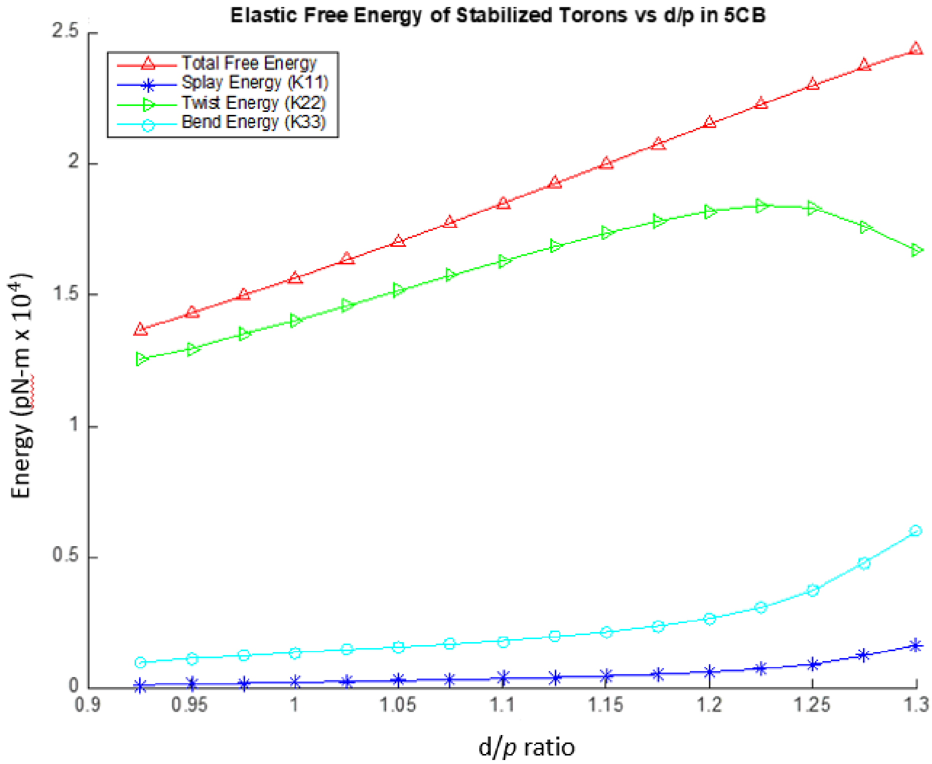

Figure 7 | A plot of simulated elastic free energy of stabilized torons vs d/*p* ratio in the 5CB nematic LC host. As in equation (1) the bend and splay energies are not related to d/*p*, while the twist free energy is directly proportional to d/*p*. As we are increasing the pitch by light exposure and hence decreasing the d/*p*, the bend and splay free energy essentially remain unchanged, and the twist free energy decreases and therefore the total free energy decreases as well. The twist energy begins to decrease above d/p = 1.2 as the configuration becomes unstable.

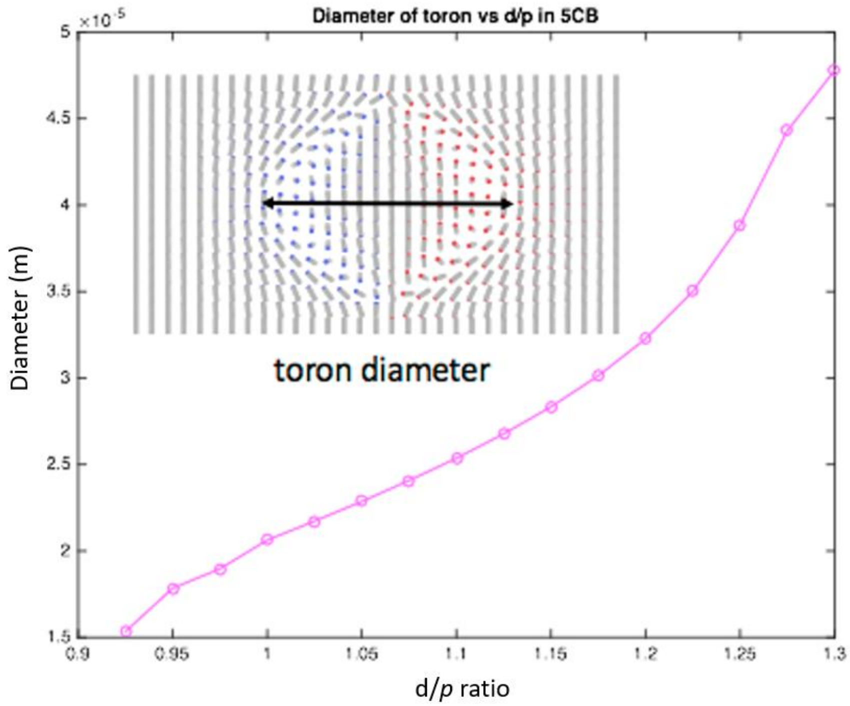

Figure 8 | A plot of simulations of toron size-dependence on d/*p* ratio in 5CB nematic base LCs. The toron diameter is directly proportional to d/*p*.

We conducted experiments in three samples with different thicknesses, d: sample IQ1 with d = 10μm, IQ2 with d = 7 μm, and sample IQ3 with d = 15 μm. In each sample a few torons were generated and pinned by optical tweezers so that it would be easier to analyze the size over time without any possible translational motions. A uniform blue light pattern was projected onto the samples IQ1 and IQ3 by the projector system connected to the Olympus BX51 microscope with a 10× dry objective to test the shrinking process of the experiment; and in IQ2 we stopped the projection after 5 different lengths of exposure time, and let the LC return to its ground state in order to test the growing back aspect of the experiment. The POM images and videos for the two processes were recorded with the CCD camera. The videos were then analyzed using the open-source software ImageJ and its plugins. For each shrinking video we chose five torons for analysis, and the extracted data sets were used to calculate speed and size changes. The growing back videos were analyzed in the same fashion.

2.2.1.2 Results

As soon as we started exposing the samples, the torons began shrinking as expected. An example of the process of the experiment can be seen in Figure 9 below. And after we took the projection away, as the cholesteric LCs began to relax, the torons slowly grew back close to their original sizes as the d/*p* increased. This process is similar but reversed compared to the exposed/shrinking part of the experiment.

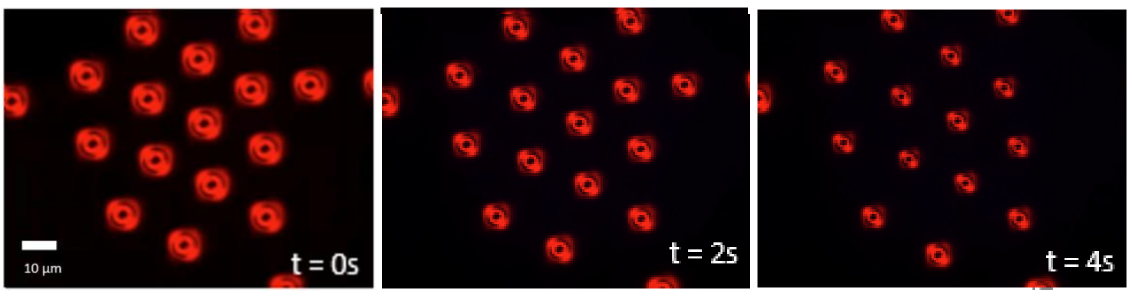

Figure 9 | POM Images of the process of the toron shrinking taken under the Olympus BX-51 microscope. The images are arranged by increasing time of exposure, and one can tell from the images that the diameters of torons decreases as exposure time increases.

For the shrinking experiments, the data analysis results of the five example torons we chose from each sample are shown in Figure 10. As seen on the graphs, the starting diameter of the torons were larger in cell IQ3, ranging from 29 µm to 32 µm, compared to 16-18 µm in IQ1. In IQ1, after approximately 5 s of exposure, the torons shrank to disappear, while in IQ3 torons could still exist after a longer period of exposure. Speed-wise, in IQ1 the torons shrank at 2.42 µm/s on average, and in IQ3 the mean speed of shrinking was 0.56 µm/s.

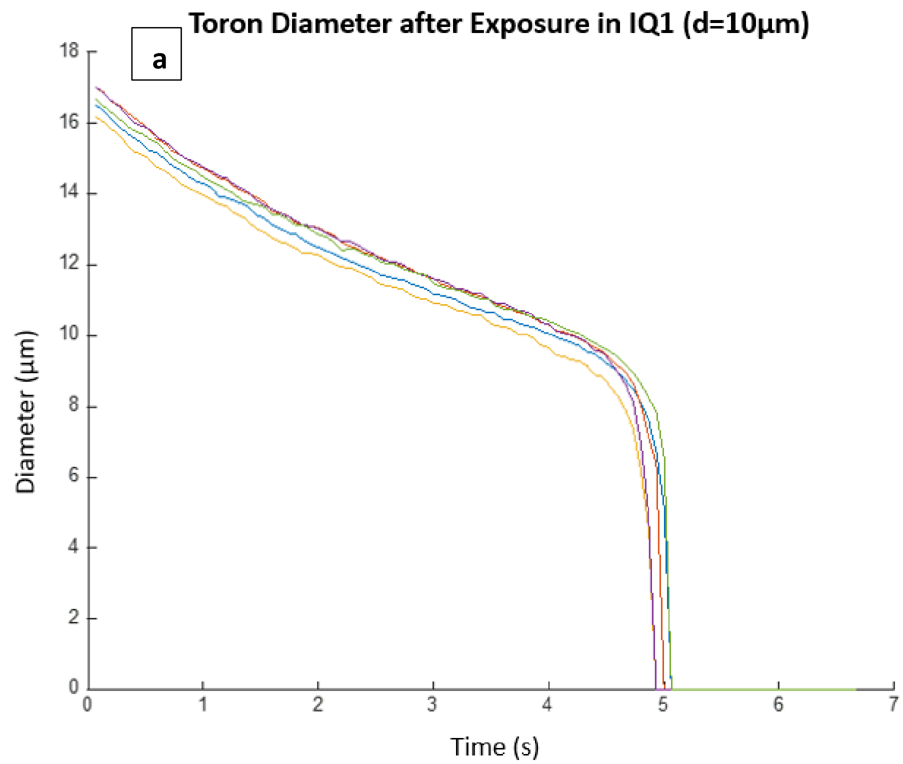
Toron Diameter after Exposure in IQ1 (d=10µm)
a
Diameter (µm)
Time (s)
18
16
14
12
10
8
6
4
2
0
0
1
2
3
4
5
6
7

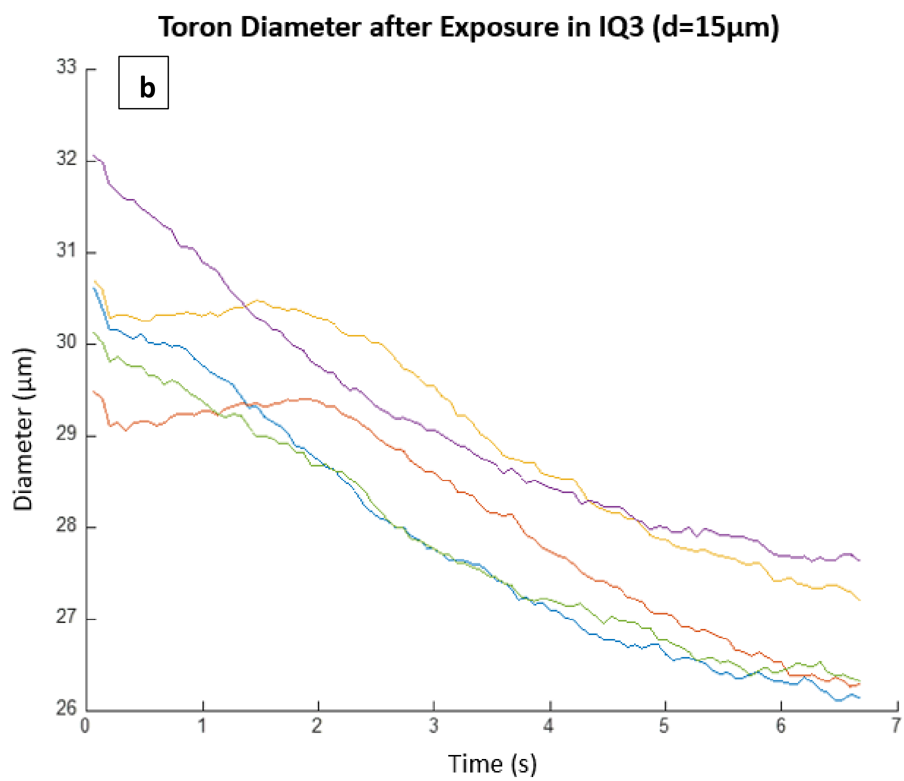
Toron Diameter after Exposure in IQ3 (d=15µm)
b
Diameter (µm)
Time (s)
33
32
31
30
29
28
27
26
0
1
2
3
4
5
6
7

Figure 10 | (**a**) A plot of toron diameter vs. time in sample IQ1, d = 10 μm and p = 10 μm. Different color denotes different torons. (**b**) A plot of toron diameter vs. time in sample IQ3, d = 15 μm and p = 15 μm. Different color denotes different torons. Note the starting sizes of the torons in the two samples are different.

For the growing back experiments, the result of the analysis of five different exposure times is shown in Figure 11. As expected, the starting size of the torons of the growing back experiments are inversely proportional to the exposure time. The time the torons took to grow back to the original sizes were roughly 700 s, which is significantly longer than the shrinking process. As a result, the speed of growing back was also much smaller, approximately 0.009 μm/s.

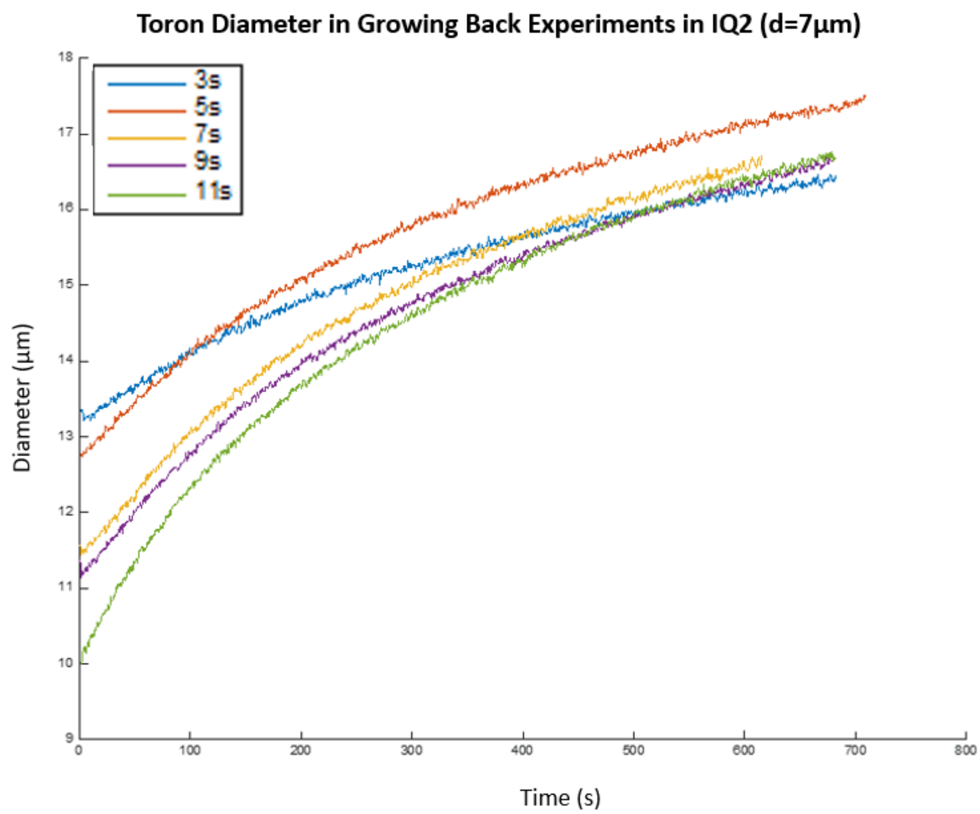

Figure 11 | A plot of toron diameter vs. time for the toron growing back experiments in sample IQ2, d = 7 μm. Different color denotes different starting size. Since the sizes of torons are dependent on the exposure time based on Figure 10, the smaller the post-exposure starting size, the longer the toron was exposed.

In conclusion, based on our observations, the torons do have size-dependence of the d/*p* ratio as expected. The starting size of torons is larger in thicker cells, and usually these torons shrink at a lower speed but can endure longer exposures, while in thinner cells torons shrink faster and disappear after a certain amount of exposure, which means they react faster and are more delicate. Finally, after exposure, the system needs a much longer time to get back to its ground state.

2.2.2 Toron Controllable Directional Motions

2.2.2.1 Experiments

Since a basic understanding of the nature of torons' reaction to light-induced pitch changes in the QL76 Cholesteric LC samples was established, a series of toron controllable directional motion experiments were designed and tested. As I have mentioned several times in this paper, torons tend to move to regions that have the original d/*p* ratio (d/*p* ~ 1) to avoid changes. Therefore, inducing a gradient in pitch, or experimentally exposing the sample with patterns of projection (instead of uniform exposure), would in principle cause the torons to move. In addition, because different patterns can be projected onto different positions of the cells, the motions of torons induced should also be controllable. Combined with the conclusion from the uniform exposure experiments, when a toron is experiencing gradient change in pitch of the surroundings, or in other words the toron is not entirely confined in the pattern of projection, it would shrink its size to fulfill twist energy while moving away from the exposed region, hence controllable directional motion.

Non-uniform exposure patterns with light and dark regions were projected by the projecting system connected to the BX51 microscope. The patterns to be projected onto the samples were put in PowerPoint slides on a laptop computer that was connected to the projector (See Fig.12), and control of toron motions was made possible by switching to different slides with different patterns or by manipulating the projecting system to alter the position of a projection.

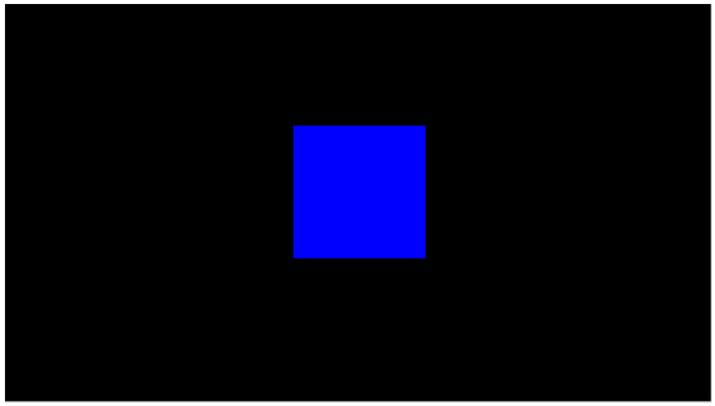

Figure 12 | A simple example of the slides we used to project to the sample. The pattern to be projected in blue light is the blue square in the middle, and its surrounding were painted black to minimize disturbance.

2.2.2.1.1 “Shuttle Run” Motion

The “Shuttle Run” motion experiment was the first attempt to induce a motion with light projection. The goal of the experiment was to demonstrate that the direction of linear motion of torons could be controlled by different light patterns. For this experiment, a toron was generated using the optical tweezer apparatus in sample IQ1 (d = 10 μm), a bar-shaped blue pattern was then projected onto the sample, covering 1/3 to 1/2 the size of the toron to induce the initial motion of the toron. Different slides with different locations of the bar-shaped projection were used during the process of the motion to push the toron farther. After a certain desired distance had been reached, a bar-shaped pattern was projected in front of the toron in the initial direction of motion, therefore theoretically the toron would gradually stop and change the direction of motion. Figure 13(a) shows the process of the experiment. The video of the experiment taken by the CCD camera was analyzed in ImageJ to track the motion of the toron. The extracted data was then processed in MATLAB to get the trajectory and speed of the motion (see Figure 13 (c) and (d)).

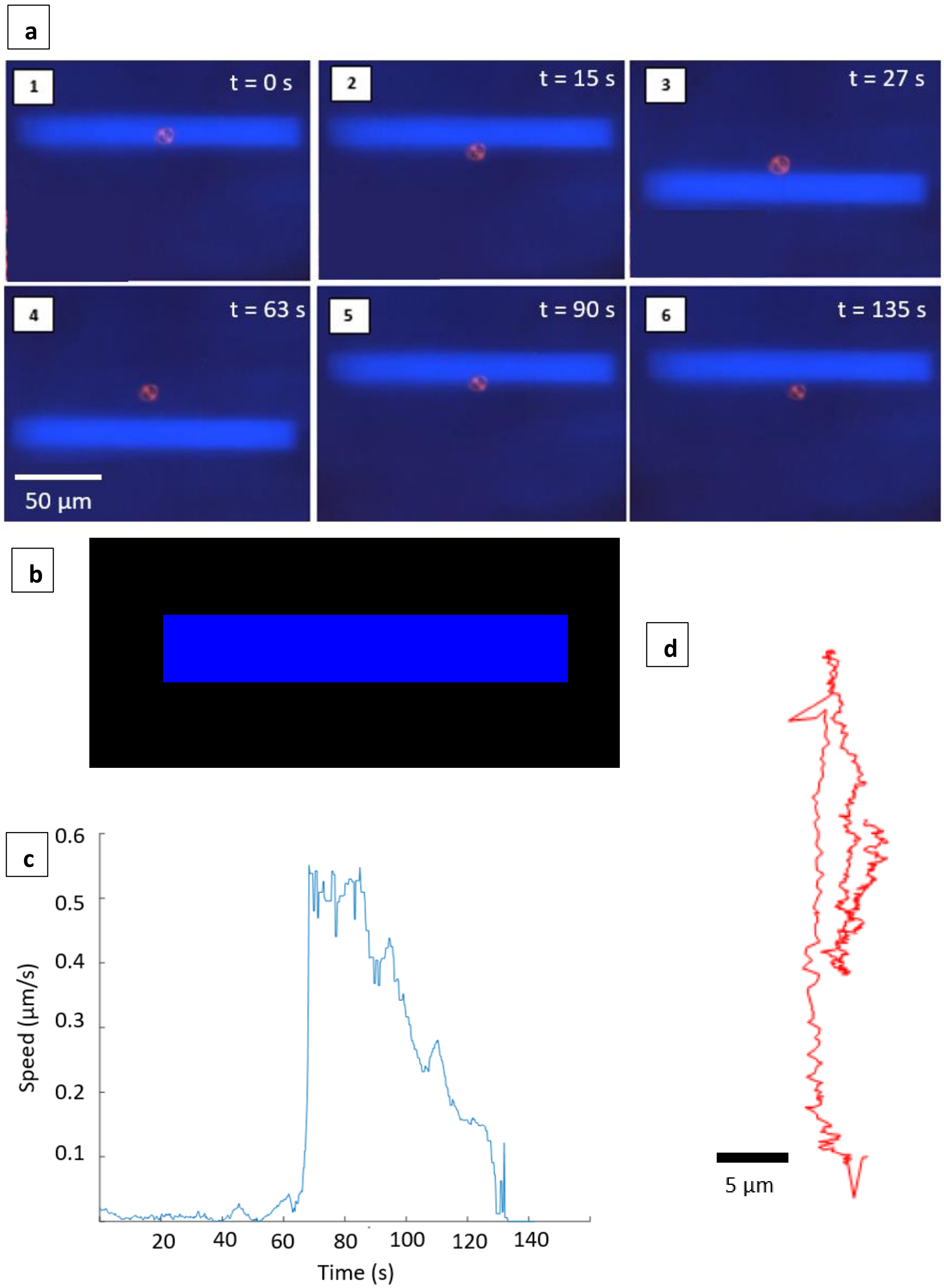
a
1
t = 0 s
2
t = 15 s
3
t = 27 s
4
t = 63 s
5
t = 90 s
6
t = 135 s
50 µm
b
d
5 µm
c
0.6
0.5
0.4
0.3
0.2
0.1
Speed (µm/s)
20
40
60
80
100
120
140
Time (s)

Figure 13 | (a) A series of images from the video recorded of the "Shuttle-Run motion" experiment. Picture 1~6 are aligned in time sequence. The toron was exposed in picture 1 and started moving downwards and in picture 3 it was slowed down by the projection in the direction of the initial motion, and in picture 4 it started moving upwards, slowed down by projection in 5, and started moving downward in 6. (**b**) One of the slides of the pattern used in the experiment. The pattern remained the same throughout the experiment with different locations on slides, hence different projecting positions on the sample to induce or slow down the toron motion. (**c**) Speed of the toron motion. (**d**) Trajectory of the motion of the toron.

As expected, the toron switched the direction of motion, which indicated that controlling the dynamics with light patterns and specifically changing the direction of linear motion was possible. An interesting phenomenon was discovered during the experiment: the toron was intended to be controlled to repeat the "Shuttle-Run" several times, yet after the toron changed direction, the velocity of the toron decreased, and was eventually unable to be moved after a second downward "push". Based on Figure 13(c), the maximum speed occurred right after the sample was been exposed, and then continuously dropped until the toron stopped moving. This phenomenon continued to affect the experiments later, and will be discussed further in the following sections.

2.2.2.1.2 Complex Trajectories: "CU"

It was shown in the last section that toron linear directional motions can be induced and controlled with light exposure in QL76-doped CNLCs. The goal of the complex trajectory experiments is to improve the previous test and demonstrate that long distance 2D motions with turning directions (in this case less than 180 degrees) can be achieved with light patterns. And since we are a research group from the University of Colorado Boulder (CU), we decided that the best complex trajectory to start with was a "CU" logo-lookalike (Fig.14(b)). Like previous experiments torons were generated using optical tweezers and the tests were conducted using the projecting system connected to the BX51 microscope. Various methods and designs of experiments were tested during the exploration as we began to understand the nature of the dynamics.

2.2.2.1.2.1 Confined Path Patterns

Because of the nature of toron's reaction to changes in d/*p* ratio, as we have discussed several times, if there were blue light projections in one region, the region would be avoided by torons. In other words, the toron would not go into the exposed region. The very first approach arose from this concept that if a pattern was designed such that it reserved a confined track for the test toron to go through by having blue projections outside of the path, the only energetically favorable trajectory that a toron could choose, when an additional block of projection was "pushing" behind it, would be the premade track (See Fig.14(c)).

Figure 14 | (**a**) A "CU" logo of University of Colorado Boulder. (**b**) The desired CU-logo-lookalike trajectory of toron motion. (**c**) The initial pattern projected to the sample. The blue areas are blue light when projected and the dark areas are non-exposed regions. A distinctive dark shape confined in a blue square can be recognized in the figure. The width of the C track is close to 1.5 times the diameter of a toron in a d = 10 μm sample. The blue circle on the top left is designed to "push" the toron. When the experiment started, a toron was pre-positioned on the right of the circle, and as the toron moved along the C track, different slides were put on with the unchanged C track, but the circle moved along the track, following the toron to maintain constant motion.

The patterns were controlled by a PowerPoint slide on a laptop computer connected to the projecting system, and different slides were modified and projected on as the toron moved in order to steer the dynamics. As shown in Figure 14(c) above, the circle was designed to move along with the toron to force it to keep moving within the C-shaped track made by the surrounding blue patterns. After the "C" has been completed, the toron would move forward a bit and then be confined in a half-U-shaped pattern, which was designed in the same fashion with a new circle pattern behind it to "push" it along the new track, and eventually complete a whole U-shaped trajectory that denotes the formation of a "CU". Theoretically this method is very ideal because we could preset the track to be as fine as we wanted, so that the trajectory could be considerably smooth.

Unfortunately, the experimental result was not quite satisfying. Testing of the patterns were conducted in samples IQ1~4, and in each experiment, the toron motion stopped somewhere before completing the "C" shape. After regrouping and brainstorming, the method was slightly adjusted. This time instead of a complete confined "C" or "U" track throughout the experiments, segments of the confined path patterns were used (see Fig.15(a)). Although by using smaller patterns, the fineness of the resulting trajectory would unavoidably be worse, yet the benefit of the adjusted method was that whenever a toron was inside a smaller chunk of exposure, it would see a larger unexposed region in front compared to the original method, therefore it would be energetically more favorable for the toron to keep moving, and that should ideally resolve the problem we had earlier.

POM images of one of the experiments are shown in Figure 15(b). As designed, the toron was pushed all the way through the "C" pattern, however, the "U" pattern was never completed as the toron eventually stopped somewhere inside the “U” track. The videos of the experiment were analyzed as stated in section **2.2.2.1**. The results are shown in Figure 15(c) and 15(d).

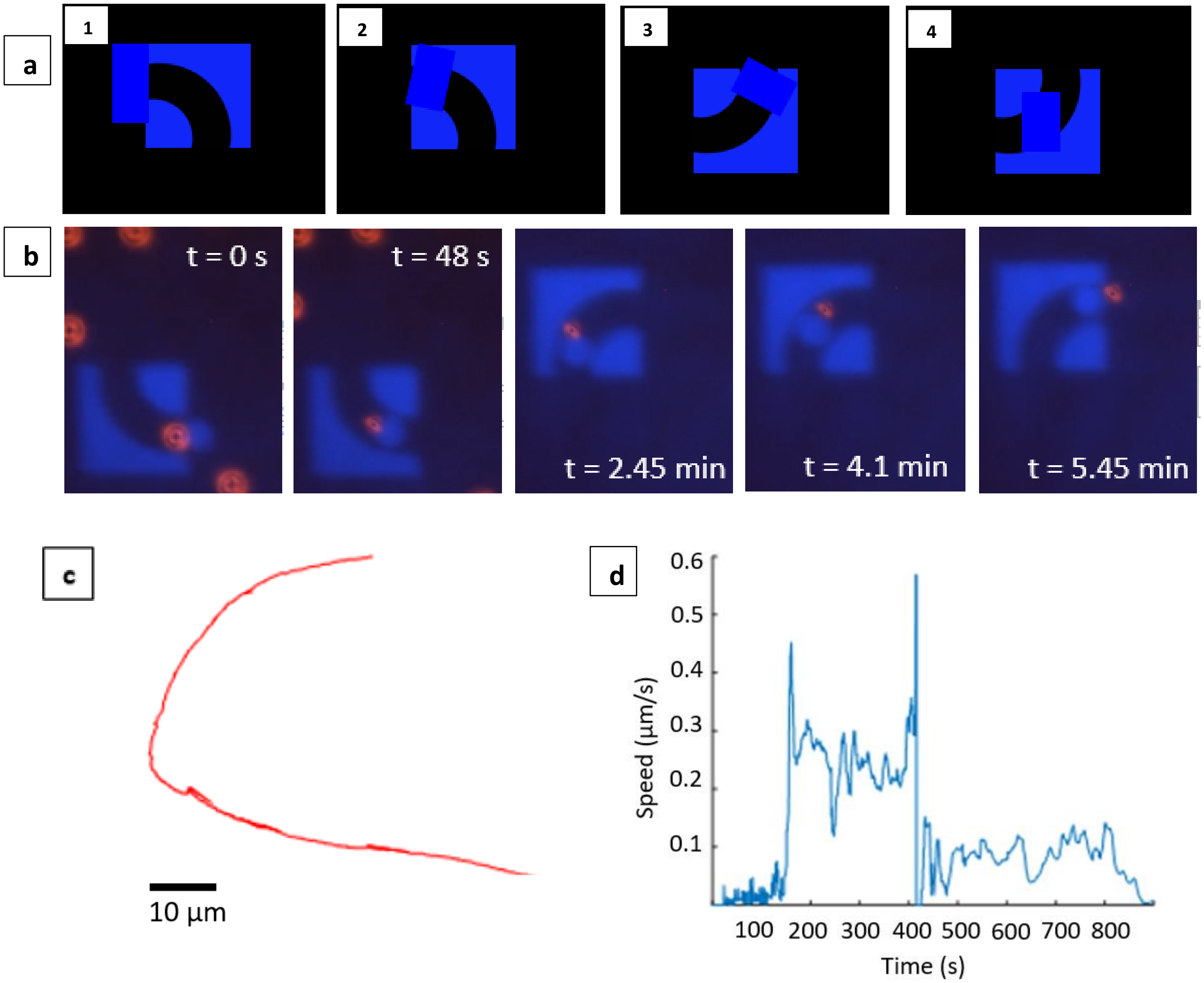

Figure 15 | (**a**) A series of sample segments of the confined path patterns. For instance, in (1), a toron was pre-positioned at the right of the rectangular shape on the upper left so that it could run away to the right into the track, as it moved farther pattern (2) was put on to give the toron another “push”. After the toron had completed the segment of path in (1) and (2), it was then confined in the lower part of the “C” track in (3), and the timing to switch from (3) to (4) as the toron moved along the track was similar. (**b**) A series of images from the video recorded of one of the “Segmented Confined Path Pattern ‘CU’ Trajectory” experiments, aligned in time sequence. In this particular experiment, the “C” trajectory was reversed, and the “pushing pattern” was a circle instead of a rectangular like in (a). Yet the physics behind are same. (**c**) The trajectory plot of the toron. (**d**) The speed plot of the toron.

It is clear the design of the tests was on the right track because we had a decent “C”. Yet the problem of the toron not completing the trajectory was not resolved but essentially delayed. At this point, it has been demonstrated that not only 1D linear toron dynamics but 2D trajectories of torons that associate with steering the direction can be controlled with light projections. The next step was to find a reproducible way to get the toron to move in the desired manner while overcoming the stopping issue.

2.2.2.1.2.2 "Pushing" Projection Only

Various methods were tested since the Confined Patterns failed, yet they all resulted in toron stopping in the middle of the tests. In the end it came to our realization that when running the experiments, diffusion of energy had not been considered. As we expose the sample with light even within a small area, we are changing the energy landscape of the cell, and diffusion of energy is inevitable as the system tries to adjust to the new state. In previous cases, e.g. the attempt to create a "CU" trajectory, the patterns were continuously exposing the area of projection, thus the diffusion of the exposure effect was happening ceaselessly. When the energy diffusion affected the area near the projection (part of the desired path) such that even the unexposed regions have the same d/p ratio as the exposed regions, the torons stopped moving since there was nowhere else more energetically favorable, just like they were experiencing uniform exposure as described in Section **2.2.1**.

With the above conclusion in mind, we decided to keep things simple: In order to minimize the effect of diffusion and saturation by light, instead of using any fancy patterns, a simple rectangular-shaped pattern of the size of a toron was used to "kick" the toron, and the direction of the motion induced depended on the part of the toron being exposed (see Fig.16). The basic track and rough positions that needed exposure were marked on the computer monitor that the CCD camera was connected to. After the initial movement, whenever we wanted to change the direction of the motion, the two knobs of a reflecting mirror on the projecting system that controls the position of the projection on the sample were used to move the projection so that it could "push" the toron once again in the desired direction. In addition, the exposure time was limited to avoid diffusion, and the environmental factor has been considered as well, therefore, these experiments were conducted in a dark room to avoid any influence other than the projection.

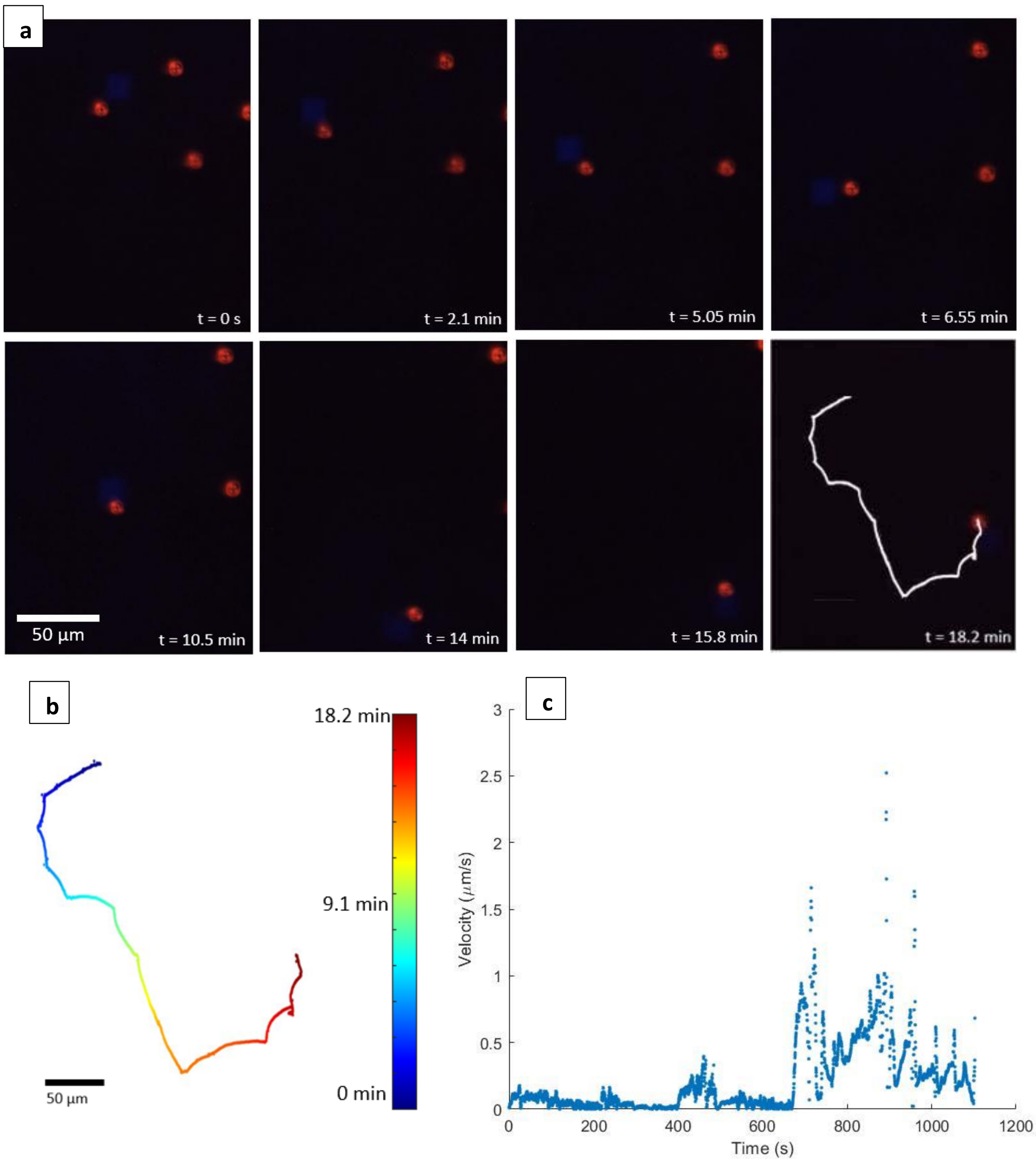

Figure 16 | (**a**) A series of images from the video recorded of the "'Pushing' Projection Only 'CU' trajectory" experiments, aligned in time sequence. The top four images represent the formation of the "C" trajectory; the bottom four images represent the formation of the "U" trajectory. The direction of the toron motion was controlled by the relative position between the toron and the projection. For instance, in the top left image, the projection is on the upper right of the toron, therefore the direction of the induced motion should be pointing to the lower left direction, opposite of the projection position. A trajectory of the toron motion was marked on the last image.(**b**) A plot of toron motion trajectory. (**c**) The plot of speed of toron motion.

Based on Figure 16 (b), the method successfully yielded a complete "CU" pattern. Yet the result was not ideal because the trajectory was very rough. To demonstrate that a finer trajectory can be achieved, an additional experiment was conducted focusing on producing only a smooth "C" shape. The results are shown below.

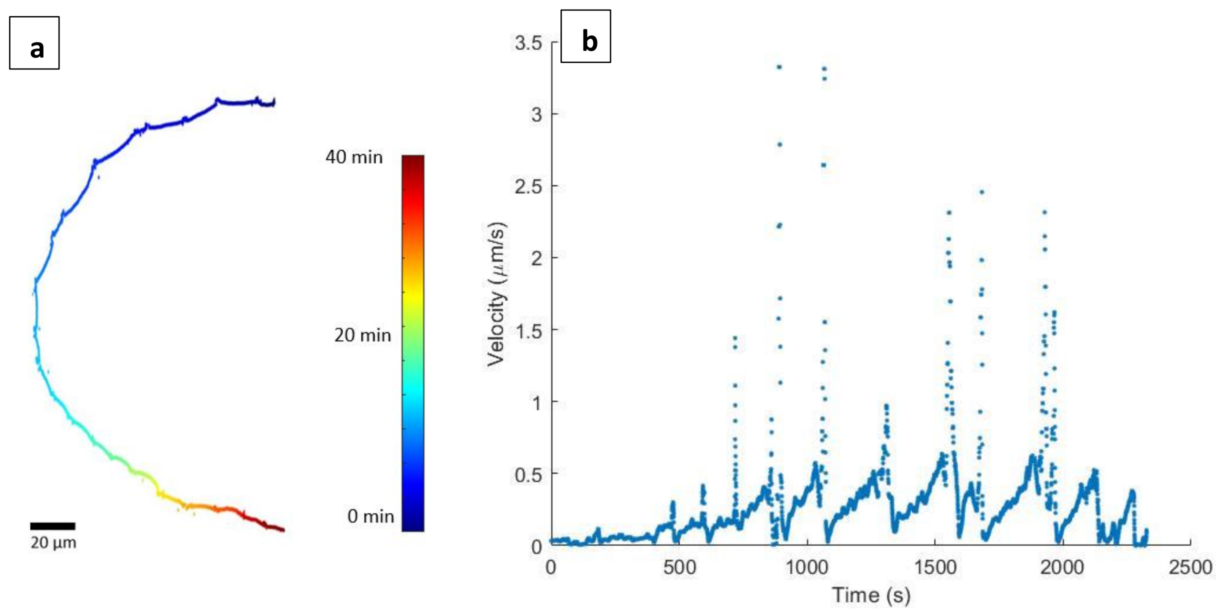

Figure 17 | (**a**) A plot of a finer C-shaped toron motion trajectory. (**b**) The plot of speed of toron motion.

It is easy to observe that the trajectory shown in Figure 17(a) is smoother and more like a typical "C" letter compared to Figure 16(b). Therefore, it is clear that the preciseness of the trajectory of toron motion can be increased. It can be concluded that toron dynamics in QL76-doped CNLCs can be controlled by minimizing both exposure time and area to form complex trajectories without being affected by diffusions of exposure effect, and that the steering techniques should be explored more to increase the smoothness of the trajectory obtained.

2.2.1.2.3 Additional Experiments

Since a “CU” is merely making a toron move from one area to another, and the “Shuttle-Run” experiments also ended with toron stopping, additional experiments are needed to demonstrate that the torons can return to their original regions once they moved away from them. Therefore, a Spiral Trajectory Test was conducted where essentially the idea was to “push” the toron to move counter-clockwise in a spiral radially outwards (into a reversed “9” shape) so that the torons could go back near the original area while having a complex trajectory. The experimental method was exactly the same as described in last section. And the experimental results are shown in Figure 18, where it is clear that the desired reversed “9”-shaped trajectory was observed.

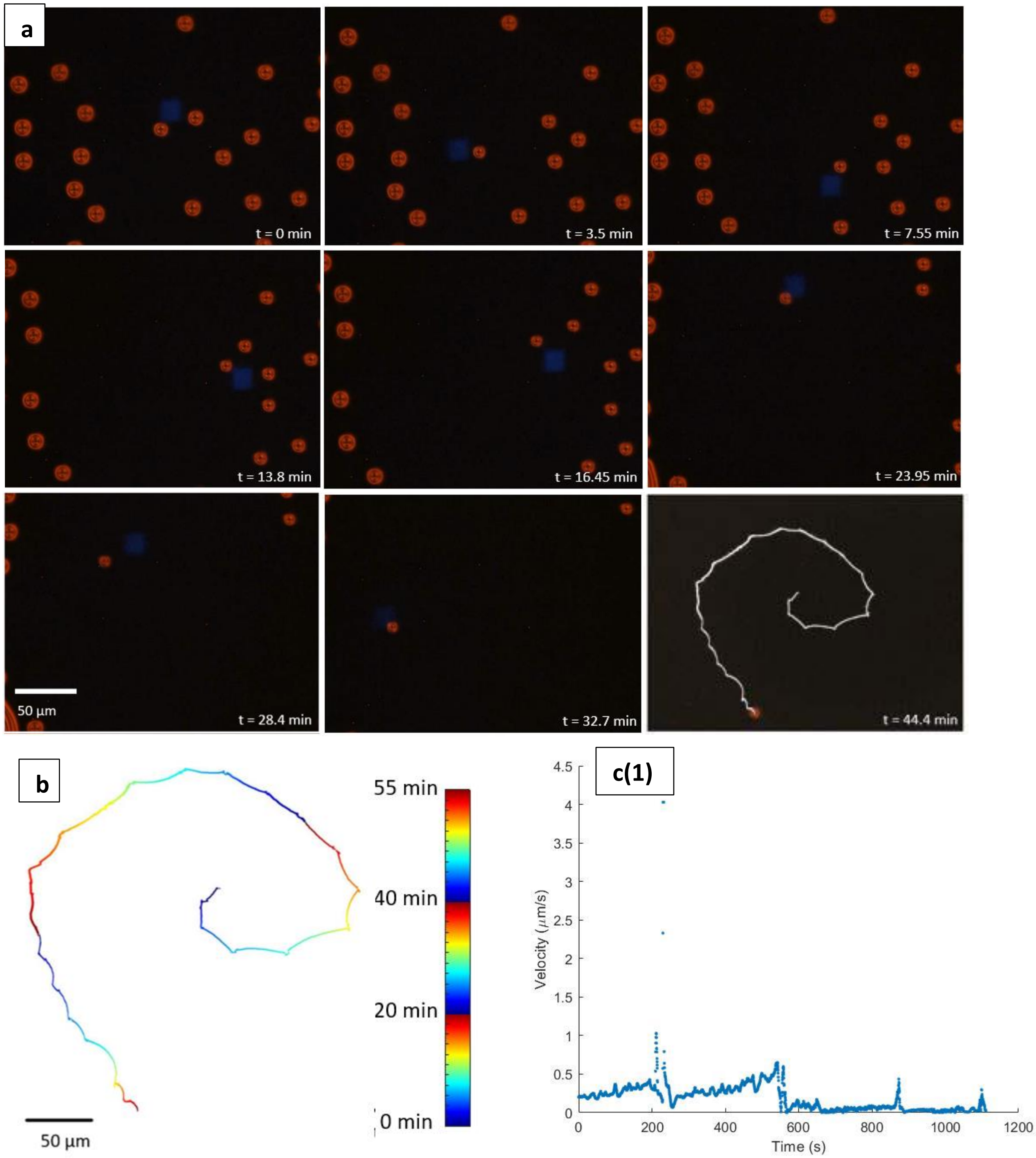
a
t = 0 min
t = 3.5 min
t = 7.55 min
t = 13.8 min
t = 16.45 min
t = 23.95 min
50 µm
t = 28.4 min
t = 32.7 min
t = 44.4 min
b
55 min
40 min
20 min
0 min
50 µm
c(1)
Velocity (µm/s)
Time (s)
0
0.5
1
1.5
2
2.5
3
3.5
4
4.5
200
400
600
800
1000
1200

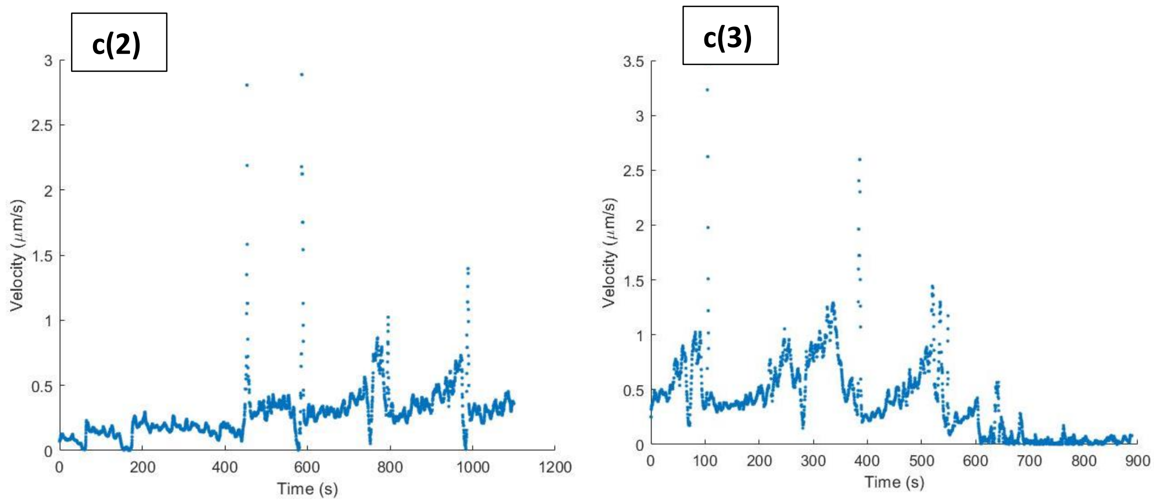

Figure 18 | (**a**) A series of images from the video recorded of the "Reversed 9-Shaped trajectory" experiments, aligned in time sequence. A trajectory of the toron motion was marked on the last image in white. (**b**) The trajectory plot of the toron motion. Note that the video was cut into three pieces and analyzed separately considering the size, the obtained three trajectories were then put together to give a clearer look of the whole picture. (**c**) The speed plots of the toron motion. Note that video was cut into 3 pieces when being analyzed considering the size, and the c(1), (2), and (3) are in time sequence, with no time gap in between.

2.2.2.2 Conclusions

We have explored and demonstrated that 1-dimentional linear motion and 2-dimentional complex trajectory of torons in QL76-doped CNLCs can be completed using light projections, which represent the photo-directed motion of torons in QL76-doped CNLCs are indeed photo-tunable.

2.2.3 Photo-tunable Toron Lattice Structure

In flat LC cells with strong surface anchoring and thickness of about 5 μm and larger as well as lateral sample thickness variations of about 1% or less, torons generated by laser beams of power of 50 mW and higher are typically immobile and can be used for long-term stable 2D lattices [16]. Previous research in our group has demonstrated that these "pinned" torons can be used to form 2D electrically erasable long-term-stable periodic crystalline lattices, which can also be dynamically modified and tailored depending on need, offering a great potential for bridging fundamental studies and applications in soft condensed matter, photonics, electro-optics, and other fields [16]. In the research hexagonal, as well as square lattices, have been proved to be generable and voltage-tunable.

Since the "unpinned" torons have been mainly studied in this project, it would be interesting to explore whether they can form tunable crystalline lattices in QL76 cholesteric LC samples like the "pinned" ones through light projection. This requires an array of torons being generated by the optical tweezer apparatus, and the basic experimental setup was the same as stated in previous sections.

2.2.3.1 Experiments

2.2.3.1.1 Hexagonal Lattices

In [16] it was also stated that mobile torons can assemble into hexagonal crystalline lattices by exploiting lateral confinement and short-range repulsive interactions. Therefore, it is necessary to test if arrays of mobile torons would self-assemble into hexagonal lattices with patterned light projection. Methodologically, the best way to demonstrate this is to push the torons together and observe the structure they form. For this purpose, two approaches were used. As shown in Figure 19(a), a solid circle pattern was projected in the middle of an array of torons, forcing the torons to move radially outwards and hence created a close structure. Another method was to project a hollow circle pattern, meaning the exposure was merely the edge of the circle as shown in Figure 19(b), pushing the torons within the circle to go inward and thus form a closed structure. The pattern was projected onto the samples briefly for a few seconds. And the analysis of the videos recorded yielded Figure 19(d) and (e).

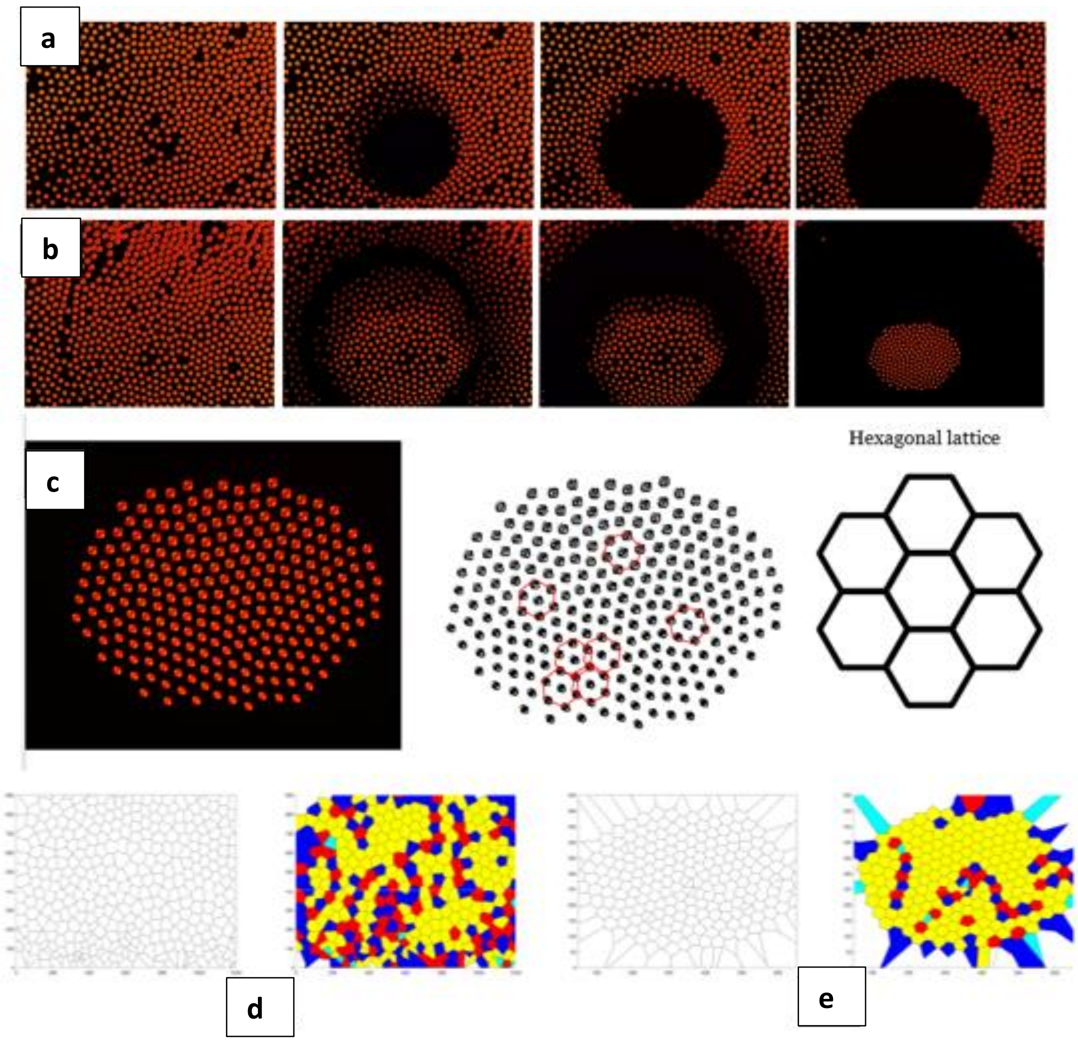

Figure 18 | (**a**) A series of screenshots of the process of projecting a solid circle pattern onto the sample, arranged in time sequence from left to right. (**b**) A series of screenshots of the process of projecting a hollow circle pattern onto the sample, arranged in time sequence from left to right. (**c**) From left to right: An enlarged picture of the final state of the arrays of torons as they were pushed together to form a closed structure; A grayscale version of the previous picture with red hexagons denoting the hexagonal crystalline structure the torons form; schematic of a typical hexagonal lattice structure. (**d**) The structures adjacent torons formed before the exposure was analyzed and color coded, yellow represents the hexagon, red represents heptagon, dark blue represents pentagon, and light blue represent square. (**e**) The structure adjacent torons form after being pushed together, with the same color code as in (d).

Based on Figure 18(d) and (e), the hexagonal shapes outnumbered the other structures for both cases of pushing the torons outwards or inwards, which proves that arrays of torons would self-assemble into a hexagonal lattice with an applied field. The next step was to explore whether arrays of mobile torons could be manipulated to form square lattices similar to pinned torons, using photo-tuning in QL76 Cholesteric LCs.

2.2.3.1.2 Square Lattices

A checkerboard pattern shown in Figure 19(a) was used to achieve the square-lattice structure of mobile toron arrays. The squares of the checkerboard pattern were adjusted to perfectly include one toron only. Theoretically, when the pattern was projected on to a relaxed self-assembled toron array with hexagonal lattice, the torons would move to the squares with no exposure, thus completing the desired structure. The experiments were conducted in sample IQ1 with d = 10 μm. As in the last section, an array of torons were generated by optical tweezers. The exposure time was long for this test in order to give the torons enough time to react to the considerably finer pattern. Experimental methods and data analysis were the same as in last section.

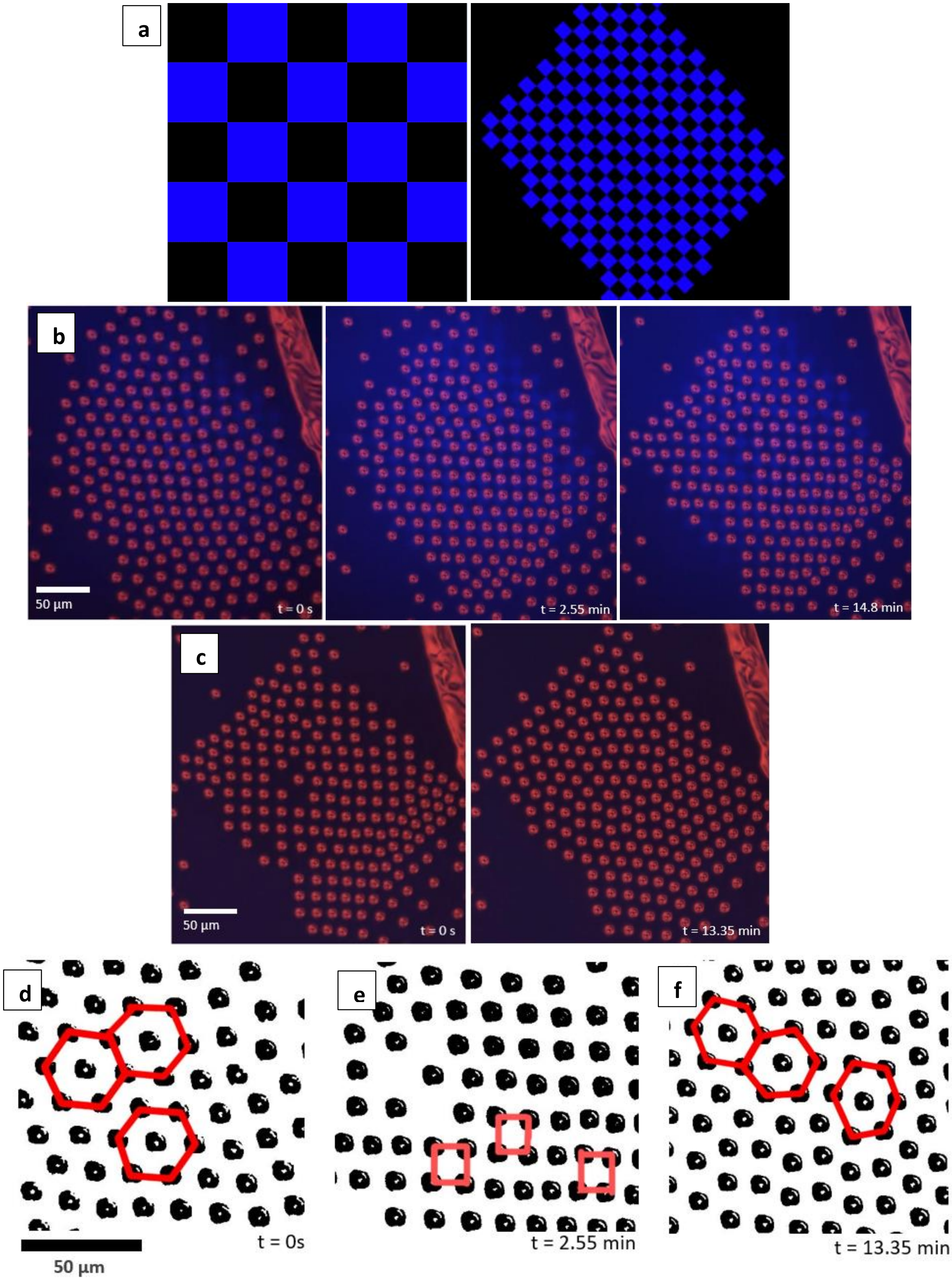
a
b
50 µm
t = 0 s
t = 2.55 min
t = 14.8 min
c
50 µm
t = 0 s
t = 13.35 min
d
e
f
t = 0s
t = 2.55 min
t = 13.35 min
50 µm

Figure 20 | (**a**) The left image is a normal checkerboard pattern. The right image is the smaller tilted checkerboard pattern used in the "Square-Lattice Formation" experiment. The checkers were designed such that they can only include one toron inside. (**b**) A series of images from the video recorded of the "Square-lattice Formation" experiment, aligned in time sequence. From left to right: the initial structure formed by the array of torons before the exposure; the first square-lattice the array of torons formed; the second square-lattice the array of torons formed after the position of the projection was slightly moved to the upper right direction. (**c**) A series of images from the video recorded of the "Lattice Relaxation" experiment, aligned in time sequence. From left to right: the initial structure of the array of torons when the exposure was taken away; the final structure of the array of torons after a period of time with no exposure. (**d**) A grayscale version of the enlarged lattice structure of the array of torons before exposure, with red hexagons denoting the hexagonal structures. (**e**) A grayscale version of the enlarged lattice structure of the second square-lattice formed, with red rectangles denoting the square structures. (**f**) A grayscale version of the enlarged final structure of the array of torons after a period of relaxation time, with red hexagons denoting the hexagonal structures.

The torons were observed to be moving as expected. The array originally formed in hexagonal structures as shown in Figure 20(d), after the exposure started, the torons realigned to move to the blank space left in the checkerboard pattern (to adjust to the changed localized d/*p* ratio)(see Fig.20(b)), resulting in the desired square-lattice structure. The structure was stable when the pattern was projected to the sample. For the purpose of testing if the structure was reproducible, the pattern was slightly moved by adjusting the reflection mirror in the projecting system connected to the Olympus BX51 microscope. As a result, the torons also realigned to the new position of the checkerboard and formed perfect square lattices (Fig.20(e)). After the projection was taken away, as the system relaxed to the ground state, the former square-lattice structured array of torons automatically realigned and formed the more energy favorable hexagonal-lattice structure (Fig.19(f)).

2.2.3.2 Conclusion

Based on the results of the experiments, it was clear that the large array of torons would automatically self-assemble to a hexagonal-lattice structure; under exposure of projected patterns, facile generation of reconfigurable and tunable square-latticed structures was observed. These experiments demonstrated that the mobile torons could have the same tunable structures in QL76 Cholesteric LCs as the pinned torons shown in [16]. It is also plausible to believe that other kinds of lattice-like structures can be achieved using different projecting patterns, meaning that more photo-tunable lattice structures of toron arrays could be explored, which would potentially broaden the application consideration of defect-enabled devices in soft condensed matter, photonics, and many other fields.

2.2.4 "Squirming" Motion under Light Exposure

2.2.4.1 Experiment

In previous research projects in my group, a modulated high-frequency electric filed was applied to the entire sample with volume 10^8 times larger than that occupied by a typical single solitonic structure. The facile response of the LC results in the strong coupling between the electric field $\mathbf{E}$ and director field $\mathbf{n}(\mathbf{r})$, causing a periodic local conversion of electric energy into the soliton's translational squirming motion, which can allow for engineering spatial translation of solitons with and without carrying cargo [12,14]. The voltage-tuning mechanisms of this directional electrically driven motion was described in detail in [14]. In this research, the "squirming" motion was also studied under light exposure by photosensitizing the voltage-tunable samples with QL76. For these experiments, we used similar samples made of MLC-6609 and QL76. After an array of torons was generated in the sample, a gated electric field around 4.0 V (square wave, 1000Hz, modulation frequency 2Hz, duty cycle 75%) was applied to the sample to induce the squirming motion; after the squirming motion started, a circle pattern was projected onto the sample for a long period of time to determine how light exposure affected the electric-driven motion.

2.2.4.2 Result

After the modulation started, the torons formed chains as they "squirmed" with the TIC (translationally invariant configuration, induced by the voltage tuning, see [14]) as expected. With the projection presenting, as time went on, the chains of torons tended to avoid going into the region of light exposure just like in usual QL76-doped CNLC samples we used for the experiments described earlier (see Fig.21). This result implies that the principle concepts of photo-tuning still hold even when the sample has on applied electric field. Therefore, various ways of photo-tuning the electric-driven "squirming" motion of torons can be explored further to achieve precise control of the motion, which would ultimately broaden application consideration.

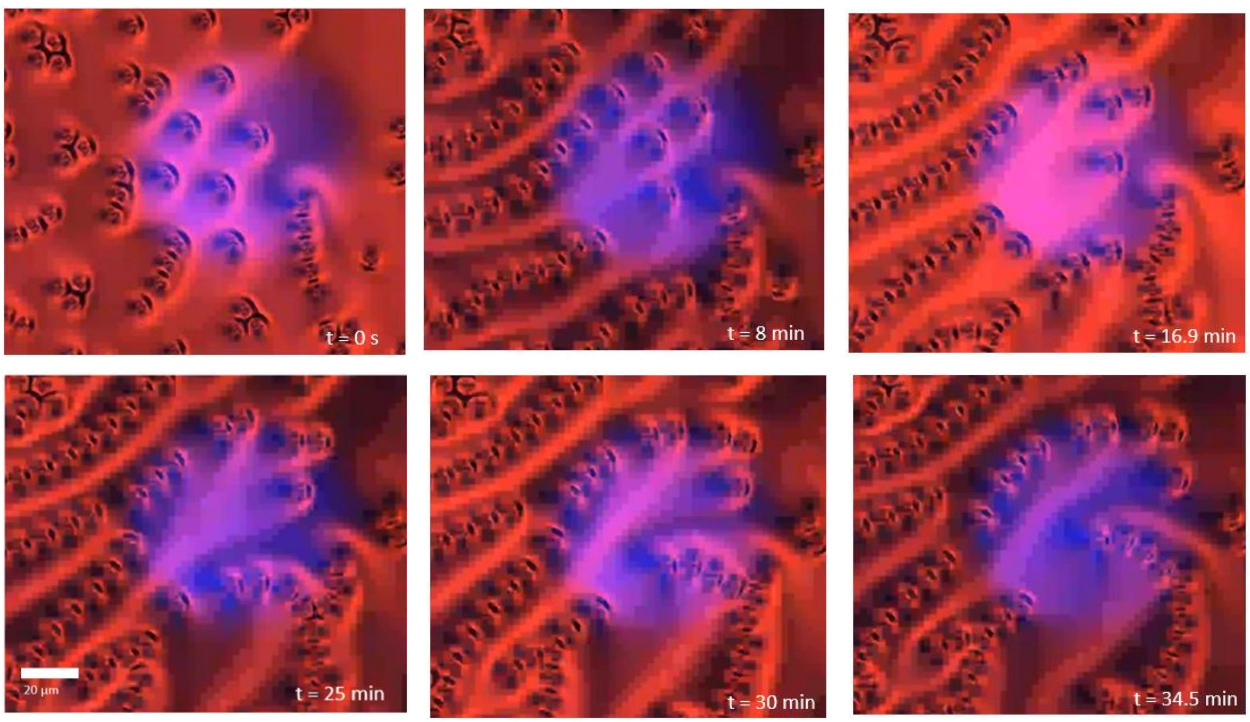

Figure 21 | A series of screenshots of a series of images from the video recorded of the "'Squirming' Motion under Light Exposure" experiment, aligned in time sequence.

3. Conclusion and Discussion.

In conclusion, in QL76 CNLCs, topological solitonic structures called torons (1) change size to fulfill twist free energy when exposed to uniform light projection, and (2) exhibit a directional photo-driven motion when exposed to a gradient light projection. It has been demonstrated that precise control of the motion is possible using patterns of projection as steering tools.

As stated earlier, solitons play an important role in a wide range of fields of physics, and are fairly accessible when using LCs as a host medium. Since the typological solitonic structures we studied – torons – have a four-fold relationship with solitons (stated in Section 1.2), the dynamic properties we discovered in this research could potentially benefit studies in many other fields. Together with other studies of torons and other topological solitons, a model system could be established for the study of out-of-equilibrium phenomena related to field transformations within condensed matter and beyond. On the other hand, photo-tunable dynamics of mobile torons could also yield new applications for CNLC devices and micro-cargo carrying techniques with a wide range of use.

We can also conclude that an array of torons can self-assemble into a hexagonal-lattice-like structure, which can be manipulated to form a reconfigurable square-lattice-like structures with blue light projection patterns. Earlier research has shown that the benefit is the robustness with which the periodic patterns of LC defects (torons) can be generated and switched, thus obtained diffraction gratings can be designed to work in both Raman-Nath and Bragg regimes [16, 17, 18]. This research furthers the study by providing a new means to generate and switch the periodic patterns of torons.

In addition, a new means of controlling the “squirming” motion of torons when applied with a gated electric field was found as the torons still try to avoid the light-exposed area, which furthers the study of “squirming” motions of torons in [14]. Combining previous work with our results, the application consideration in new electro-optic, photonic, and all-optical devices as well as new types of information displays can be expanded.

While this research serves as a first-step analysis of the photo-tunable dynamics of torons, additional work can be done. Testing different colors of patterns (which contains different polarizations and light intensities) would aid in the understanding of the speed of the photo-tunable dynamics, and thus provide new techniques for precise controlling of both the photo-directed and electric-directed motion. Finally, testing the precise control of the photo-directed motions of torons with micro-cargo carrying could also find a wide range of applications among the fields of biology and physics.

4. References

1. Senyuk, B. Liquid Crystals: A Simple View on a Complex Matter. < http://www.personal.kent.edu/~bisenyuk/liquidcrystals/intro.html>
2. Andrienko, D. Introduction to liquid crystals. <http://www2.mpipmainz.mpg.de/~andrienk/teaching/IMPRS/liquid_crystals.pdf> (2006)
3. Dierking, I. (2003). *Textures of liquid crystals*. John Wiley & Sons.
4. Fernsler, J. Liquid Crystals < http://www.calpoly.edu/~jfernsle/Research/Liquid%20Crystals/LCResearch.html>
5. Dauxois, T., & Peyrard, M. (2006). *Physics of solitons*. Cambridge University Press.
6. Moraru, L. (2014). Solitons-A Bridge between Mathematics and Physics.
7. Manton, N., & Sutcliffe, P. (2004). *Topological solitons*. Cambridge University Press.
8. Fukuda, J. I., & Žumer, S. (2011). Quasi-two-dimensional Skyrmion lattices in a chiral nematic liquid crystal. *Nature communications*, *2*, 246.
9. Murphy, A. Blue Phases in Liquid Crystals < http://guava.physics.uiuc.edu/~nigel/courses/569/Essays_Fall2011/Files/murphy.pdf>
10. Ackerman, P. J., Boyle, T., & Smalyukh, I. I. (2017). Squirming motion of baby skyrmions in nematic fluids. *Nature communications*, *8*(1), 673.
11. Ackerman, P. J., Van De Lagemaat, J., & Smalyukh, I. I. (2015). Self-assembly and electrostriction of arrays and chains of hopfion particles in chiral liquid crystals. *Nature Communications*, *6*, 6012.
12. Boyle, T. J., "Characterizing the Dynamic Properties of Toron-Umbilic Pairs" (2016). *Undergraduate Honors Theses*. 1057. https://scholar.colorado.edu/honr_theses/1057
13. Ackerman, P. J., & Smalyukh, I. I. (2017). Diversity of knot solitons in liquid crystals manifested by linking of preimages in torons and hopfions. *Physical Review X*, *7*(1), 011006.
14. Sohn, H. R., Ackerman, P. J., Boyle, T. J., Sheetah, G. H., Fornberg, B., & Smalyukh, I. I. (2018). Dynamics of topological solitons, knotted streamlines, and transport of cargo in liquid crystals. *Physical Review E*, *97*(5), 052701.
15. White, T. J., Bricker, R. L., Natarajan, L. V., Tabiryan, N. V., Green, L., Li, Q., & Bunning, T. J. (2009). Phototunable azobenzene cholesteric liquid crystals with 2000 nm range. *Advanced Functional Materials*, *19*(21), 3484-3488.
16. Ackerman, P. J., Qi, Z., Lin, Y., Twombly, C. W., Laviada, M. J., Lansac, Y., & Smalyukh, I. I. (2012). Laser-directed hierarchical assembly of liquid crystal defects and control of optical phase singularities. *Scientific reports*, *2*, 414.
17. Born, M., & Wolf, E. (2013). *Principles of optics: electromagnetic theory of propagation, interference and diffraction of light*. Elsevier.
18. See Supplemental Material at http://link.aps.org/supplemental/10.1103/PhysRevE.86.021703 for videos on laser diffraction patterns and a figure on experimental and simulation details.